

Article

Molecular Simulations of the Gas Diffusion through the Two-Dimensional Graphyne Membrane

Dongliang Jin , Tao Zhang, Meng Guo , Nanhua Wu and Jing Zhong * 

Jiangsu Key Laboratory of Advanced Catalytic Materials and Technology, School of Petrochemical Engineering, Changzhou University, Changzhou 213164, China

* Correspondence: zjwyz@cczu.edu.cn

Abstract: Owing to the unified and tunable pore size, two-dimensional graphyne membranes show excellent performance in the realm of gas transport and separations. The impacts of environmental conditions on the pore size of a porous membrane are ignored in previous studies. Using molecular modeling techniques, we here probe the accessible pore size of the γ -graphyne membrane under various pressure and temperature conditions. First, by assessing the gas permeation through the two-dimensional γ -graphyne membrane at a constant temperature, the accessible pore size of this membrane is shown to be proportional to the driving force—the pressure difference between the two sides of the porous membrane. Such a driving force dependence is found to be well described by a simple asymptotic model. Then, by determining such pressure dependence at two different temperatures, temperature is found to show a weak influence on the accessible pore size. Finally, by considering the binary mixed gases of various mole fractions, the accessible pore size measured using one of the two species is shown to be dependent on its partial pressure difference. These findings for the accessible pore size, which highlight the tunable pore size by altering the driving force, can be expected to provide a practical strategy to rationalize/refine the pore size of the porous membrane for gas transport and separations, especially for two molecules with similar diameters.

Keywords: molecular dynamics; graphyne; accessible pore size; separations



Citation: Jin, D.; Zhang, T.; Guo, M.; Wu, N.; Zhong, J. Molecular Simulations of the Gas Diffusion through the Two-Dimensional Graphyne Membrane. *Separations* **2023**, *10*, 499. <https://doi.org/10.3390/separations10090499>

Academic Editor: Victoria Samanidou

Received: 18 August 2023

Revised: 4 September 2023

Accepted: 11 September 2023

Published: 13 September 2023



Copyright: © 2023 by the authors. Licensee MDPI, Basel, Switzerland. This article is an open access article distributed under the terms and conditions of the Creative Commons Attribution (CC BY) license (<https://creativecommons.org/licenses/by/4.0/>).

1. Introduction

Graphynes are family members of two-dimensional (2D) carbon allotropes in which the acetylenic linkages (i.e., R groups) are introduced to connect the hexagons of graphene [1–3]. These linear acetylenic linkages lead to many triangular pores of a uniform accessible size d for gas permeation (Figure 1) [4,5]. Due to their high selectivity, permeability, and mechanical stability [6,7], graphynes are thought to be promising candidates as environmentally friendly porous membranes in the realm of the gas transport and separations [8–10]. For instance, the graphyne membrane with rhombus-like pores results in a high selectivity for hydrogen separation from carbonic oxide and nitrogen [11]. In particular, the accessible pore size of the graphyne membrane can be readily modified by introducing linkages with different sizes (i.e., different number of acetylenic units) [12]. For example, graphdiyne with acetylenic groups $-C\equiv C-C\equiv C-$ is shown to be preferable for hydrogen purification from syngas as its accessible pore size d is in between the molecular kinetic diameters of hydrogen σ_{H_2} and methane/carbonic oxide $\sigma_{CH_4/CO}$ (i.e., $\sigma_{H_2} < d < \sigma_{CH_4/CO}$) [13]. In contrast, the triangular pore of graphyne with acetylenic groups $-C\equiv C-$ is too small to allow hydrogen passing through [14]. Due to the tunable, tailored, or task-specific pore size, graphyne membranes receive increasing attention with significant effort devoted to better understanding the contributions of the accessible pore size to the gas transport and separations [15].

In parallel to experimental studies devoted to estimating the gas permeability of the graphyne membranes, many theoretical works have focused on the thermodynamics and

dynamics of gas transport and separations through these membranes [16]. For instance, theoretical approaches relying on molecular dynamics simulations have been employed to probe the transport kinetics of gas permeation through a porous membrane [17], while the first-principle methods have been successfully used to explore the pore size effects on the diffusion barriers and kinetics of the gas permeation through a porous membrane [18]. In these calculations, the accessible pore size d is considered to be independent of pressure, temperature, and so on. The mechanisms involved in the gas transport and separation processes have been unraveled by many thermodynamic aspects. From a fundamental point of view, the gas permeation through a porous membrane is governed by a complex interplay of several factors such as nanopore geometries [19], kinetic diameters of gas species [20], and the accessible pore size. Beyond these discussions on the mechanisms and kinetics, the effects of the complex permeation conditions such as the pressure and temperature on the accessible pore size of a porous membrane have not been considered.

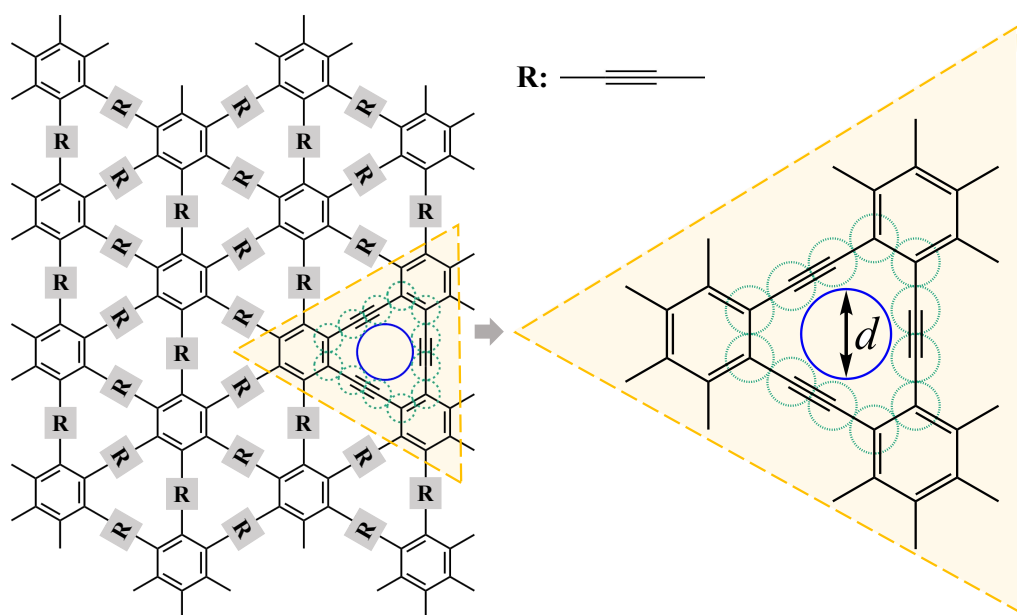


Figure 1. Image shows the molecular configuration of the two-dimensional γ -graphyne membrane. The zoom-in scheme illustrates the accessible pore size d (blue circle) formed by the van der Waals spheres (green circles) of carbon atoms (note that d is flexible).

In this contribution, we employ an effective and robust molecular modeling approach to determine the accessible pore size d of a porous membrane. This pore size is characterized using the critical molecular dynamic size that is slightly smaller than the actual pore size. Such a definition ensures that the number of confined gas molecules in pore space goes to zero as $d \rightarrow 0$ [21,22]. By considering many gas molecules with different molecular kinetic diameters, the critical molecular size that allows gas permeation through the porous membrane is determined by performing molecular dynamics simulation (we note that this approach could be easily implemented into Monte Carlo algorithms) [23]. Despite its simplicity, such a straightforward way shows the effects of the gas permeation conditions (pressure, temperature, etc.) on the accessible pore size. In addition, this molecular approach could be extended to other porous materials. This work aims to provide a molecular approach to estimate the accessible pore size of a 2D porous membrane, therefore neglecting the chemical, structural, and mechanical aspects on the gas transport and separation. For example, graphene oxide membranes modified using various functionalized groups show a more effective CO_2/N_2 separation performance compared to graphyne membrane [24,25].

The remainder of this article is organized as follows. In Section 2, we present the computational details: molecular system, interaction potentials, and molecular dynamics

(MD) simulations in the canonical ensemble. In Section 3, using our molecular approach, we present the important results regarding the impacts of environmental conditions on the accessible pore size of a porous membrane. First, relying on the diffusion/transport of a single-component gas, we determine the accessible pore size of the two-dimensional γ -graphyne membrane under different driving forces—the pressure difference between two sides of the membrane. The scaling between the accessible pore size and the driving force is shown to be well described using an asymptotic model. Then, we discuss the effects of temperature on the accessible pore size. The pressure dependence is shown to be weakly influenced by temperature. Finally, the asymptotic model is validated by considering binary mixed gases instead of the pure gas. The driving force dependence is found to be independent of the partial pressures of other gas species. Section 4 presents some concluding remarks.

2. Materials and Methods

The two-dimensional γ -graphyne membrane is described as a rigid porous framework (Figure 1). In this molecular configuration, the bond lengths l_{CC} of the delocalized π bond (for benzene), the single bond, and the triple bond (for alkyne) are taken as $l_{CC} = 0.142$ nm, 0.154 nm, and 0.120 nm, respectively. Figure 2 schematically illustrates the molecular systems used to determine the accessible pore size of the 2D γ -graphyne membrane. The axes of the pores of the 2D membrane are set up to be aligned to the z -axis, and all carbon atoms are positioned at $z = 0.0$ nm (i.e., the center of the simulation cell). The left side (i.e., the region with -20.0 nm $< z < 0.0$ nm) of the γ -graphyne membrane is filled with a number of gas molecules, therefore forming a high-density phase. This high-density phase consists of either a single-component gas (Figure 2a) or a binary mixture (Figure 2b), and the total number of gas molecules is N_g . Two reflective walls are placed at $z = -20.0$ nm and 20.0 nm, respectively, so that the gas molecules do not migrate to the vacuum layers (i.e., the regions with $z < -20.0$ nm or $z > 20.0$ nm). This implies that if a gas molecule moves outside the wall on a timestep by a distance δ , then it is put back inside the face by the same δ , and the sign of the corresponding component of its velocity is flipped [26]. In doing so, the gas molecule could diffuse from one side to the other through the porous membrane rather than the cell boundary. The dimensions of the simulation cell are $L_x \sim 12.2$ nm, $L_y \sim 11.6$ nm, and $L_z \sim 50.0$ nm, respectively.

For the 2D γ -graphyne membrane, there is no intramolecular interaction included as we consider a rigid framework. Each carbon atom/gas molecule is modeled as a Lennard–Jones (LJ) interaction site. The gas–gas and gas–membrane interactions are described using the LJ(12,6) potential:

$$u_{ij}(r_{ij}) = 4\epsilon_{ij} \left[\left(\frac{\sigma_{ij}}{r_{ij}} \right)^{12} - \left(\frac{\sigma_{ij}}{r_{ij}} \right)^6 \right], \quad (1)$$

where r_{ij} is the separation distance between two atoms ij . ϵ_{ij} and σ_{ij} are the LJ interaction parameters. The LJ parameters of carbon atom of the γ -graphyne membrane are $\epsilon_{CC} = 0.058$ kcal/mol and $\sigma_{CC} = 0.343$ nm [27]. The LJ parameters of the gas molecule are $\epsilon_{AA} = \epsilon_{BB} = 0.200$ kcal/mol while σ_{AA} and σ_{BB} ; they depend on subsequent molecular simulations. The subscripts, including A and B, correspond to the two species in a binary mixture. The LJ parameters between unlike atoms are obtained using the Lorentz–Berthelot mixing rules: $\epsilon_{ij} = (\epsilon_{ii}\epsilon_{jj})^{1/2}$ and $\sigma_{ij} = (\sigma_{ii} + \sigma_{jj})/2$. In all our molecular simulations, the LJ interaction potentials are truncated beyond a cut-off of $r_c = 1.400$ nm.

All the molecular dynamics (MD) simulations are performed using the LAMMPS simulation package (stable release 23 June 2022) [28]. The equation of motion is integrated using the velocity Verlet algorithm with a timestep of 2 fs. Starting from initial molecular configurations, the canonical (i.e., constant number of molecules N , constant volume V , and constant temperature T) ensemble MD simulation is performed for 100 ns to observe the transport of the gas molecules through the γ -graphyne membrane. Temperature is

controlled using the Nosé–Hoover thermostat with a typical relaxation of 200 fs [29,30]. Periodic boundary conditions (PBC) are applied in the x - and y -directions, while the z -axis is constrained in these MD simulations.

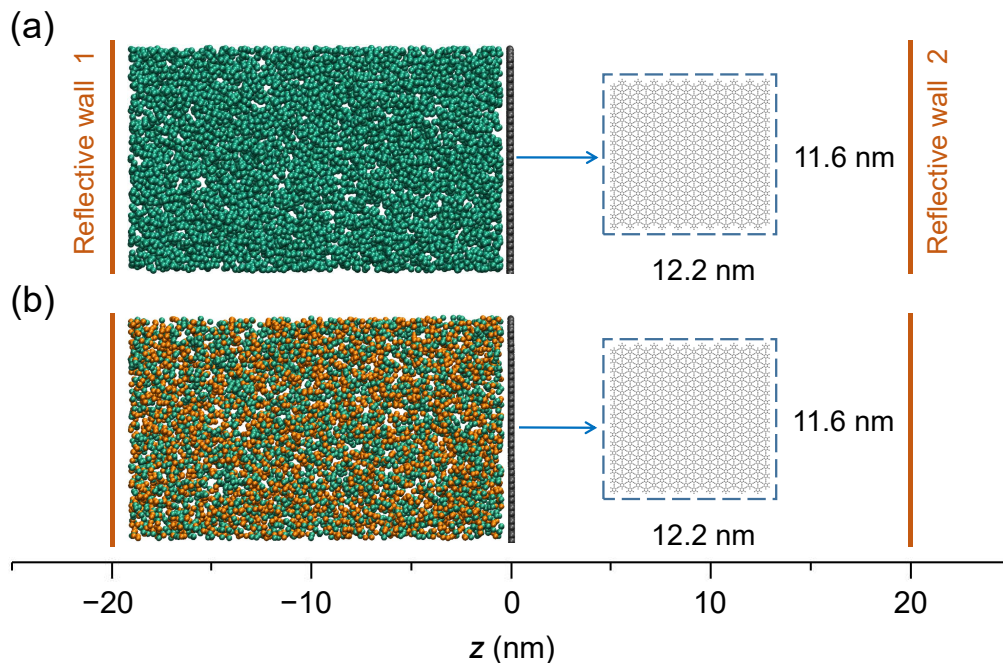


Figure 2. Molecular images show the simulation cells considered to determine the accessible pore size d of a porous membrane using a single-component gas (a) and a binary mixed gas (b). The porous membrane is positioned at $z = 0.0$ nm, and the axes of the pores of this membrane are aligned to the z -axis. The gray spheres are for carbon atoms of the LJ parameter σ . The green and orange spheres are for two species (A and B) of different LJ parameters (σ_A and σ_B). Reflective walls are positioned at $z = \pm 20.0$ nm. The dimensions of the simulation cells are $L_x = 12.2$ nm, $L_y = 11.6$ nm, and $L_z = 50.0$ nm, respectively. Periodic boundary conditions are applied in the x - and y -directions while the length of the simulation cell is constrained along the z -axis.

3. Results and Discussions

Figure 1 shows the molecular configuration of the 2D γ -graphyne membrane completely consisting of carbon atoms. These carbon atoms can be regarded as many van der Waals spheres of radius r , therefore leading to an accessible pore of size d , as illustrated in the zoom-in scheme of Figure 1. Note that the accessible pore size corresponds to a maximum molecular kinetic diameter that enables this gas molecule to penetrate a porous membrane. Despite the fact that a rigid porous framework is considered for gas transport and the separation processes, the accessible pore size is still thought to be alterable by controlling temperature and pressure. This is due to the fact that the atom–atom interactions show a soft potential such as the LJ potentials. In what follows, relying on the molecular modeling techniques, we probe the accessible pore size of this 2D γ -graphyne membrane by considering a varied molecular diameter of gas (i.e., the LJ parameters σ_A and σ_B). Note that σ_A and σ_B are normalized to the LJ parameter of the carbon atom (i.e., $\sigma = 0.343$ nm).

Figure 2a illustrates the molecular approach to investigate the accessible pore size d of the 2D γ -graphyne membrane. In the simulation cell, the carbon atoms of this 2D membrane are located at $z = 0.0$ nm, and the axis of the pores is aligned with the z -axis. The left side of the membrane is in contact with a gas reservoir with high pressure p_h while the right side of the membrane is in contact with a gas reservoir with low pressure p_l . The pressure difference $\Delta p = p_h - p_l$ between the two gas reservoirs is positive (i.e., $\Delta p > 0$). In other words, the region with $z < 0.0$ nm is occupied with a high-density gas phase while the region with $z > 0.0$ nm is occupied with a low-density gas phase.

Two reflective walls are positioned at $z = -20.0$ nm and 20.0 nm, respectively, to prevent the mixing of the two reservoirs through the boundary of the simulation cell. Obviously, this system is maintained in an unphysical fashion and depending on the LJ parameter σ_A of gas molecule used in subsequent molecular dynamics (MD) simulations. For a given Δp , the gas molecules diffuse from the high-density reservoir to the low-density reservoir for $\sigma_A < d$ while the gas molecules are confined between the reflective wall and the 2D γ -graphyne membrane for $\sigma_A > d$. For the initial molecular configuration, we create a vacuum reservoir for the region with $z > 0.0$ nm (i.e., $p_l \sim 0$ bar for the low-density gas phase); therefore, $\Delta p = p_h$ can be readily modified by adjusting the density of gas in the high-density reservoir. Moreover, we assume that the gas phase considered in this work behaves like an ideal gas so that the pressure p of a reservoir obeys the ideal gas law: $pV_g = N_g k_B T$ where V_g is the volume occupied with the gas reservoir while N_g is the number of gas molecules in the reservoir. $k_B T$ is the thermal energy. Similarly, this simulation cell is also used to determine the accessible pore size d for a binary mixture of two gas species (A and B), as shown in Figure 2b. A few gas molecules of species A in the high-density phase are replaced with the gas molecules of species B, therefore leading to a binary mixture consisting of species A and B. The corresponding LJ parameters of the two species are σ_A and σ_B .

Using the molecular modeling approach, we here probe the accessible pore size d of the 2D γ -graphyne membrane for a single-component gas completely consisting of the species A. Figure 3a shows the density distribution $\rho(z)$ of the gas molecule along the z -axis for temperature $T = 300$ K and initial pressure difference $\Delta p \sim 95$ bar. For the initial molecular configuration (i.e., $t = 0$ ns), this Δp corresponds to a homogeneous density $\rho \sim 76$ mg/cm³ in the region with $z < 0.0$ nm and $\rho \sim 0$ mg/cm³ in the region with $z > 0.0$ nm (black line, Figure 3a). For each Δp and T , the LJ parameters σ_A of the gas molecule range from 0.300σ to 0.450σ with an interval of 0.001σ . Starting from this initial molecular configuration, $M = 16$ MD simulations in the canonical ensemble are performed to determine the critical LJ parameter (i.e., the accessible pore size) that allows the gas diffusion through the 2D membrane. Figure 3a shows the simulation results for several representative LJ parameters $\sigma_A = 0.300 \sigma, 0.420 \sigma$, and 0.421σ where $\sigma = 0.343$ nm. On the one hand, the gas molecules diffuse from the high-density phase to the low-density phase for $\sigma_A \leq 0.420 \sigma$. As expected, the density ρ decreases in the region with $z < 0.0$ nm while ρ increases in the region with $z > 0.0$ nm (blue and red lines, Figure 3a). For instance, for $\sigma_A = 0.300 \sigma$, the density ρ on the left side of the 2D γ -graphyne membrane decreases to 53 mg/cm³ while ρ on the right side of this membrane increases to 23 mg/cm³ (blue line, Figure 3a). It should be emphasized that gas diffusion is found to be inefficient. As the pressure difference Δp decreases with gas diffusion, the driving force for the gas diffusion decreases. As a result, many long MD simulations with $t \sim 5$ ns are not sufficient to lead to a homogeneous density profile on both sides of the 2D membrane. On the other hand, the gas molecules are confined between the reflective wall and the 2D membrane (green line, Figure 3a). The above descriptions suggest that the accessible pore size d is between 0.420σ and 0.421σ for $\Delta p \sim 95$ bar. This value, which is in good agreement with the simulation data relying on the density functional theory, shows that the accessible pore size of the γ -graphyne membrane is approximated to 0.17 nm [31]. In addition, a condensed film with a higher density than the bulk is observed for each density profile. This is due to the fact that many gas molecules are adsorbed on the surface of the 2D γ -graphyne membrane owing to the weak attractive gas-carbon interactions [27,32,33]. We note that these gas molecules are also absorbed in the vicinity of the pore surface (i.e., internal structure of the graphyne), but they are technically difficult to be identified for a porous membrane with single-layer atoms.

Figure 3b shows the density profile $\rho(z)$ of gas molecules along the z -axis for $T = 300$ K and $\Delta p \sim 24$ bar. We note that this Δp corresponds to $\rho(z) \sim 20$ g/cm³ with $z < 0$ made for the initial molecular configuration (black line, Figure 3b). Results for a few representative LJ parameters, $\sigma_A = 0.370 \sigma$ (blue line), 0.398σ (red line), and 0.400σ (green line), are shown

in Figure 3b. These data show that $d = 0.399 \pm 0.001 \sigma$ for $\Delta p \sim 24$ bar, which is smaller than the value measured for $\Delta p \sim 95$ bar. This result, which is in qualitative agreement with experimental data on the gas transport through a porous membrane, suggests that increasing the driving force (i.e., the pressure difference between the two sides of the porous membrane) contributes to enhancing the flux of a fluid (either gas or liquid). According to the kinetic theory, the molar flux of a gas fluid $H = \Gamma \times \omega$ can be expressed as the number Γ of gas molecules colliding with the porous wall multiplied by the probability ω that a gas molecule has enough velocity to diffuse through the pore. For a specific gas species, at a given temperature T , Γ writes: $\Gamma = p\Lambda/h$ where Λ is the thermal de Broglie wavelength with h the Planck constant. As a result, these descriptions lead to $H = p\Lambda\omega/h$ [8,11,34]. This equation implies that the flux of fluid is enhanced when the driving force Δp increases, therefore supporting the experimental data available.

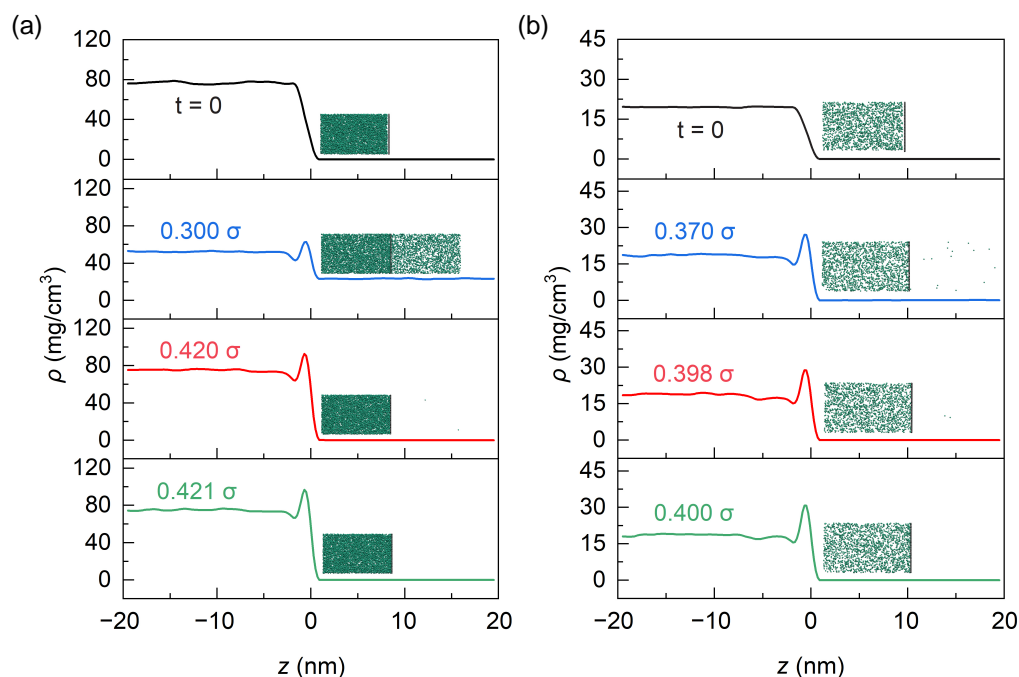


Figure 3. Density of gas ρ as a function of the z coordinates for temperature $T = 300$ K under pressure difference $\Delta p = 95$ bar (a) and 24 bar (b). Results for several representative LJ parameters σ_A are shown. Starting from the initial configuration (black line), the gas molecules penetrate the 2D γ -graphyne membrane for $\sigma_A < d$ (blue line), while these gas molecules are confined between the porous membrane and the reflective wall for $\sigma_A > d$ (red and green lines).

In the above, our simulation results show that the accessible pore size d of the 2D γ -graphyne membrane strongly depends on the driving force Δp . To probe such a dependence, we here employ the above molecular approach to measure the accessible pore size for $\Delta p \sim 47, 71, 118,$ and 142 bar (note that results for $\Delta p \sim 24$ and 95 bar are shown in Figure 3, as described previously). Figure 4 shows the accessible pore size d as a function of the pressure difference Δp . It is observed that d increases as Δp increases, simultaneously. This dependence, which shows the scaling between the accessible pore size d and the pressure difference Δp for a given temperature T , can be quantitatively described using a simple asymptotic model: $d(\Delta p) = d_\infty - (d_\infty - d_0)J^{\Delta p}$ where d_∞ is the asymptote (i.e., d proceeds to d_∞ as $\Delta p \rightarrow \infty$) [35]. d_0 corresponds to the accessible pore size owing to the complete thermal diffusion under $\Delta p = 0$. $d_\infty - d_0$ is the response range by varying Δp from 0 to ∞ . J donates the varying rate of d responsible for the pressure effect. Moreover, we assess the effects of temperature on this pressure dependence. For a given Δp , d decreases as T increases (comparison between the orange and blue data in Figure 4). This may raise concerns about the quantum tunneling effect when considering the gas transport through

the 2D porous membrane. The 2D γ -graphyne membrane is so thin that the quantum tunneling contributes to gas diffusion across a potential free energy barrier. Around room temperature, low temperature facilitates the enhancement of the tunneling effect, therefore leading to an increased accessible pore size [36–38]. It was observed that the impact of temperature on the accessible pore size becomes less significant as the pressure difference increases. The transport barriers decrease exponentially as the driving force increases and the pore size increases as well. As a result, the temperature effect on such small transport barriers can be ignored [11].

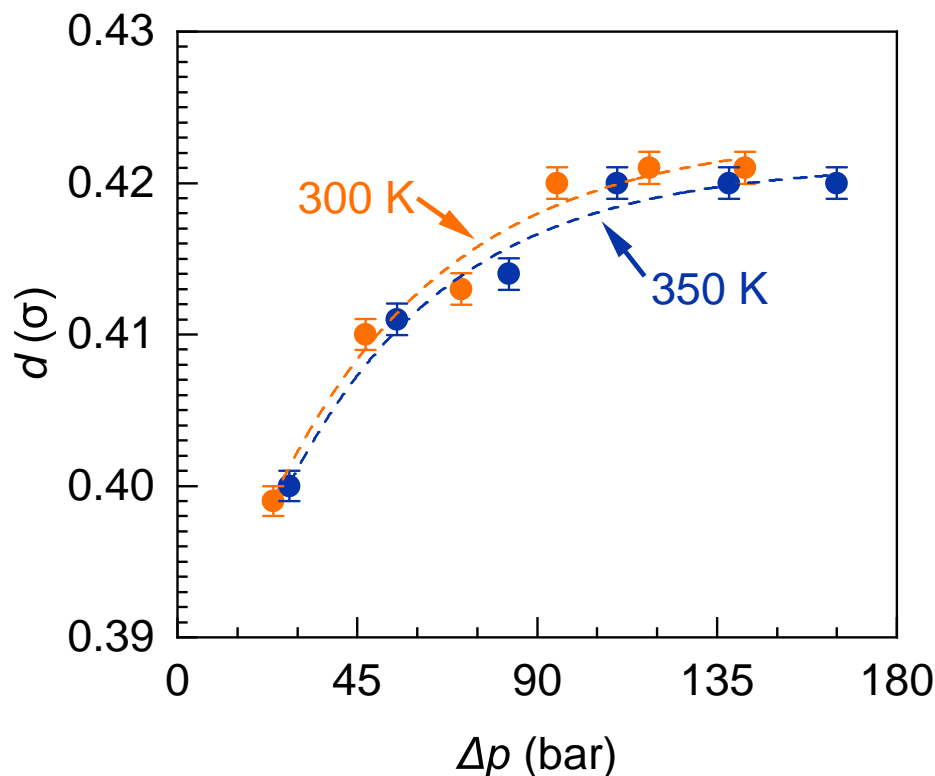


Figure 4. Accessible pore size d as a function of the pressure difference Δp for two temperatures: $T = 300$ K (orange circles) and 350 K (blue circles). The dashed lines correspond to the asymptotic model by fitting against: $d(\Delta p) = d_\infty - (d_\infty - d_0)J^{\Delta p}$.

In order to establish the scaling between the accessible pore size and the pressure difference, the single-component gas is replaced with a binary mixture (Figure 2b). In this molecular configuration, the species A is taken as the pure gas (green spheres) used in the above measurements while the LJ parameter of this species is chosen as a value larger than its asymptote. In this work, $\sigma_A = 0.430 \sigma$ is considered so that the gas molecules of species A do not migrate to the right side of the 2D γ -graphyne membrane. We here consider the following mole fractions x_B of species B (orange spheres): $x_B = 0.1, 0.3, 0.5, 0.7,$ and 0.9 . As we assumed that these gas molecules behave like an ideal gas, the partial pressure p_B of species B reads: $p_B = x_B p$ where p is the total pressure of the reservoir. For the binary mixture, the driving force is the partial pressure difference Δp_B between the two sides of the porous membrane rather than the total pressure difference Δp . This is demonstrated later by comparing the accessible pore size as a function of Δp_B and that of Δp . Figure 5a shows the density distribution $\rho(z)$ of gas molecules of the species B along the z -axis under initial partial pressure difference $\Delta p_B \sim 47$ bar (here, $x_B = 0.5$ and $\Delta p \sim 95$ bar). For the initial molecular configuration (i.e., $t = 0$ ns), this Δp_B corresponds to homogeneous density $\rho_B \sim 40 \text{ mg/cm}^3$ in the region with $z < 0.0$ nm and $\rho_B \sim 0 \text{ mg/cm}^3$ in the region with $z > 0.0$ nm (black line, Figure 5a).

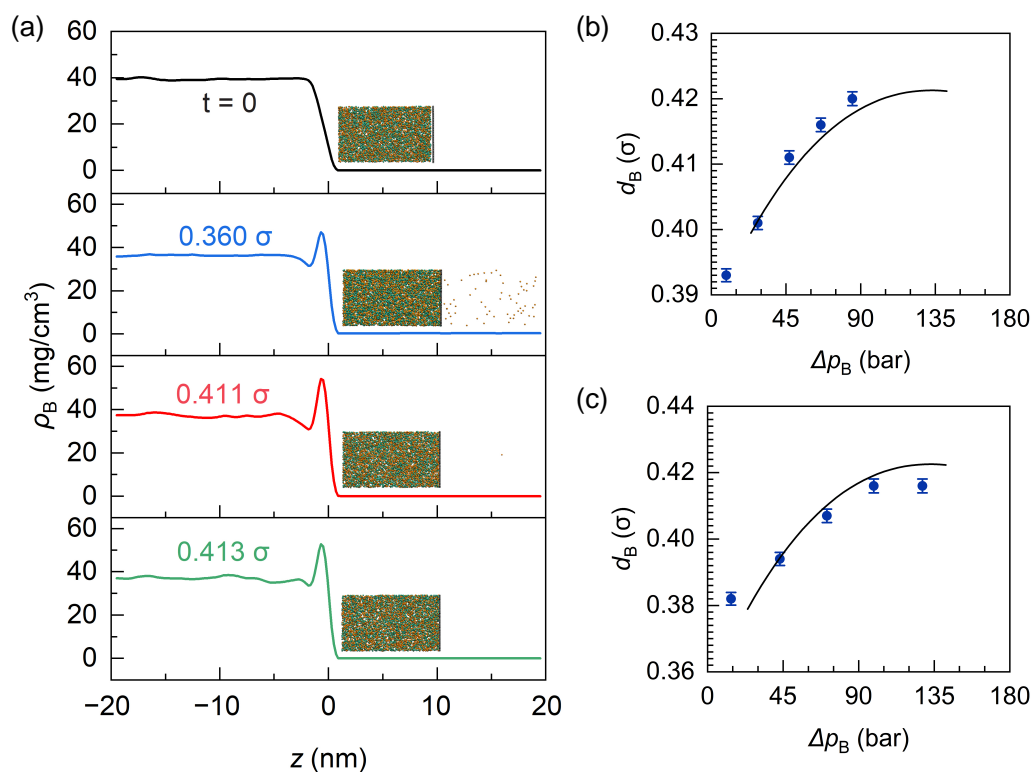


Figure 5. (a) Density ρ_B of the species B as a function of the z coordinates for temperature $T = 300$ K under partial pressure difference $\Delta p_B = 47$ bar (total pressure difference $\Delta p = 95$ bar, initial total density $\rho = 80$ mg/cm³, and mole fraction of the species $x_B = 0.5$). The green and orange spheres correspond to the species A and B, respectively. Under $\Delta p = 95$ bar (b) and 142 bar (c), accessible pore size d_B as a function of the partial pressure difference Δp_B are shown. The black solid line is for $d(\Delta p)$ obtained using an interpolation method (Figure 4) at $T = 300$ K.

Starting from the initial molecular configuration (Figure 5a), several MD simulations in the canonical ensemble are performed to determine accessible pore size d . Results for several representative LJ parameters $\sigma_B = 0.360 \sigma$ (blue line), 0.411σ (red line), and 0.413σ (green line) at temperature $T = 300$ K are shown in Figure 5a. On the one hand, the gas molecules diffuse from the high-density phase to the low-density phase for $\sigma_B \leq 0.411 \sigma$. As expected, the density ρ_B decreases in the region with $z < 0.0$ nm while ρ_B increases in the region with $z \geq 0.0$ nm (blue and red lines, Figure 5a). On the other hand, the gas molecules are confined between the reflective wall and the 2D membrane for $\sigma_B \geq 0.413 \sigma$ (green line, Figure 5a). These data suggest that the accessible pore size $d_B = 0.412 \pm 0.001 \sigma$ for $\Delta p_B \sim 47$ bar if used with the binary mixture (results for other Δp_B are shown in Figures S1–S4, Supplementary Materials). This value is comparable with the accessible pore size d obtained using the single-component gas for $\Delta p \sim 47$ bar. In order to provide a more quantitative picture of the accessible pore size as a function of the driving force, we perform a more detailed analysis in which d and d_B are extracted. Figure 5b,c show the accessible pore size as a function of the driving force for initial pressure difference $\Delta p \sim 95$ bar and ~ 142 bar, respectively. Both $d(\Delta p)$ and $d_B(\Delta p_B)$ are shown here. The line for $d(\Delta p)$ is obtained by interpolating the originated data (orange circles, Figure 4). The agreement between the single-component gas and the binary mixed gases (comparison between the circles and solid lines, Figure 5b,c) implies that the determination of the accessible pore size is independent of other species of a gas mixture. In other words, regardless of the temperature effects, the accessibility of a porous membrane is determined by the partial pressure of the targeted gas molecule so that we can completely ignore other gas species.

Despite these results, there is a number of aspects that were not considered explicitly in our approach. First, in this work, we employ the ideal gas law to estimate the pressure of a gas phase, and this assumption is only valid for low-pressure and high-temperature domains. For a high-density gas or liquid phase, developing an accurate equation-of-state to estimate the pressure/chemical potential is required [39]. Second, the pressure difference Δp between the two sides of the two-dimensional membrane was not maintained at a constant value in the molecular simulations. In these simulations, many gas molecules diffuse from the left side to the right side of the porous membrane, the pressure of the high-density reservoir decreases (i.e., $p_h \downarrow$) while the pressure of the low-density reservoir increases (i.e., $p_l \uparrow$). As a result, Δp decreases with the evolution of the molecular system (i.e., $\Delta p \downarrow$). When the simulation system reaches equilibrium, Δp vanishes (i.e., $\Delta p \rightarrow 0$ for $t \rightarrow \infty$). This molecular approach could be easily improved by using two pistons instead of two reflective walls to keep the pressure of a gas reservoir constant [40]. Third, due to the slow diffusion and reduced driving force, the molecular system needs a long simulation time to reach equilibrium. In particular, the spherical gas molecules are used in our approach. Such gas molecular models are adequate for cylindrical pores with a few molecular sizes. Finally, the porous materials in these simulations are regarded as rigid frameworks, therefore neglecting the role of the mechanical integrity of the porous membrane. This approach can be employed for flexible porous frameworks by considering the intermolecular potentials. As a result, in some cases, such as the porous solid with a pore size larger than a few molecular sizes, the accessible pore size cannot be appropriately determined using our approach.

Despite these drawbacks, this simple method captures the driving force effects on the accessible pore size of a porous membrane. Together with much experimental data available [41], the present results support the physical validity of the enhanced flux across a porous membrane with the increase in the driving force. These are expected to raise many new discussions on the effects of the driving force on gas transport and separations. For example, together with experimental methods, our molecular approach can be extended to probe the role of the driving force on the CO₂/N₂ separation through the interlayer gallery of graphene oxide membrane [24,25].

4. Conclusions

In summary, using molecular modeling techniques, we show that the accessible pore size of the two-dimensional γ -graphyne membrane strongly depends on the driving force—the pressure difference between the two sides of a porous membrane. Although we consider the 2D γ -graphyne membrane as a rigid porous framework, its accessible pore size is found to be increased when the driving force increases. Such pressure dependence is found to conform the classical macroscopic picture as described by the asymptotic model. Moreover, our molecular simulation shows that the accessible pore size measured using the binary mixed gases is similar to that determined using a pure gas under equivalent driving forces—the pressure difference for pure gas versus the partial pressure difference for a binary mixed gas. In addition, temperature is shown to contribute to the refining of the accessible pore size of a porous membrane used for the gas transport and separation processes. Despite its simplicity, the molecular approach relying on gas diffusion proposed in this work provides one of the appropriate tools to quickly determine the accessible pore size of a porous membrane such as graphyne [42,43], carbon nanotubes [44], and organosilicon [45,46].

Supplementary Materials: The following supporting information can be downloaded at: <https://www.mdpi.com/article/10.3390/separations10090499/s1>, Figure S1. Density ρ_B of the species B as a function of the z coordinates for temperature $T = 300$ K under the partial pressure difference $\Delta p_B \sim 9$ bar; Figures S2–S4. Same as Figure S1 but for $\Delta p_B \sim 28$ bar, $\Delta p_B \sim 66$ bar, and $\Delta p_B \sim 85$ bar, respectively.

Author Contributions: Conceptualization, D.J. and J.Z.; Methodology, D.J.; Software, T.Z.; Validation, T.Z. and D.J.; Investigation, T.Z., D.J. and J.Z.; Writing—original draft preparation, T.Z.; Writing—review and editing, D.J., M.G., N.W. and J.Z.; Visualization, T.Z.; Supervision, D.J. and J.Z.; Project Administration, M.G.; Funding Acquisition, D.J., M.G., N.W. and J.Z. All authors have read and agreed to the published version of the manuscript.

Funding: This research was supported by the National Key Research and Development Program of China (2022YFB3805003), the International Joint Lab of Jiangsu Education Department, the Changzhou Sci&Tech Program (CZ20220033; CJ20220140), the National Natural Science Foundation of China (22108015), the Natural Science Foundation of Jiangsu Province (BK20210855), and a grant from Changzhou University (ZMF23020018).

Data Availability Statement: The data presented in this study are available on request from the corresponding author. The data are not publicly available due to privacy.

Acknowledgments: The authors thank the Advanced Catalysis and Green Manufacturing Collaborative Innovation Center for their support.

Conflicts of Interest: The authors declare no conflict of interest.

References

1. Haley, M.M. Synthesizing γ -graphyne. *Nat. Synth.* **2022**, *1*, 413–414. [[CrossRef](#)]
2. Li, Z.; Smeu, M.; Rives, A.; Maraval, V.; Chauvin, R.; Ratner, M.A.; Borguet, E. Towards graphyne molecular electronics. *Nat. Commun.* **2015**, *6*, 6321. [[CrossRef](#)]
3. Hu, Y.; Wu, C.; Pan, Q.; Jin, Y.; Rui, L.; Martinez, V.; Huang, S.; Wu, J.; Wayment, L.J.; Clark, N.A.; et al. Synthesis of γ -graphyne using dynamic covalent chemistry. *Nat. Synth.* **2022**, *1*, 449–454. [[CrossRef](#)]
4. Drahushuk, L.W.; Strano, M.S. Mechanisms of gas permeation through single layer graphene membranes. *Langmuir* **2012**, *28*, 16671–16678. [[CrossRef](#)]
5. Ozmaian, M.; Fathizadeh, A.; Jalalvand, M.; Ejtehadi, M.R.; Allaei, S.M. Diffusion and self-assembly of C₆₀ molecules on monolayer graphyne sheets. *Sci. Rep.* **2016**, *6*, 21910. [[CrossRef](#)]
6. Zheng, J.J.; Zhao, X.; Zhao, Y.; Gao, X. Two-dimensional carbon compounds derived from graphyne with chemical properties superior to those of graphene. *Sci. Rep.* **2013**, *3*, 1271. [[CrossRef](#)]
7. Sajjad, M.; Nair, S.S.; Samad, Y.A.; Singh, N. Colossal figure of merit and compelling HER catalytic activity of holey graphyne. *Sci. Rep.* **2023**, *13*, 9123. [[CrossRef](#)]
8. Sun, C.; Bai, B. Gas diffusion on graphene surfaces. *Phys. Chem. Chem. Phys.* **2017**, *19*, 3894–3902. [[CrossRef](#)]
9. Sun, C.; Boutilier, M.S.; Au, H.; Poesio, P.; Bai, B.; Karnik, R.; Hadjiconstantinou, N.G. Mechanisms of molecular permeation through nanoporous graphene membranes. *Langmuir* **2014**, *30*, 675–682. [[CrossRef](#)]
10. Du, H.; Li, J.; Zhang, J.; Su, G.; Li, X.; Zhao, Y. Separation of Hydrogen and Nitrogen Gases with Porous Graphene Membrane. *J. Phys. Chem. C* **2011**, *115*, 23261–23266. [[CrossRef](#)]
11. Zhang, H.; He, X.; Zhao, M.; Zhang, M.; Zhao, L.; Feng, X.; Luo, Y. Tunable Hydrogen Separation in sp–sp² Hybridized Carbon Membranes: A First-Principles Prediction. *J. Phys. Chem. C* **2012**, *116*, 16634–16638. [[CrossRef](#)]
12. Shi, L.; Xu, A.; Pan, D.; Zhao, T. Aqueous proton-selective conduction across two-dimensional graphyne. *Nat. Commun.* **2019**, *10*, 1165. [[CrossRef](#)] [[PubMed](#)]
13. Cranford, S.W.; Buehler, M.J. Selective hydrogen purification through graphdiyne under ambient temperature and pressure. *Nanoscale* **2012**, *4*, 4587–4593. [[CrossRef](#)] [[PubMed](#)]
14. Owais, C.; James, A.; John, C.; Dhali, R.; Swathi, R.S. Selective Permeation through One-Atom-Thick Nanoporous Carbon Membranes: Theory Reveals Excellent Design Strategies! *J. Phys. Chem. B* **2018**, *122*, 5127–5146. [[CrossRef](#)]
15. De Oliveira, R.B.; Borges, D.D.; Machado, L.D. Mechanical and gas adsorption properties of graphene and graphynes under biaxial strain. *Sci. Rep.* **2022**, *12*, 22393. [[CrossRef](#)]
16. Tao, Y.; Xue, Q.; Liu, Z.; Shan, M.; Ling, C.; Wu, T.; Li, X. Tunable hydrogen separation in porous graphene membrane: First-principle and molecular dynamic simulation. *ACS Appl. Mater. Interfaces* **2014**, *6*, 8048–8058. [[CrossRef](#)]
17. Wang, Y.; Yang, Q.; Li, J.; Yang, J.; Zhong, C. Exploration of nanoporous graphene membranes for the separation of N₂ from CO₂: A multi-scale computational study. *Phys. Chem. Chem. Phys.* **2016**, *18*, 8352–8358. [[CrossRef](#)]
18. Mehio, N.; Dai, S.; Jiang, D.E. Quantum mechanical basis for kinetic diameters of small gaseous molecules. *J. Phys. Chem. A* **2014**, *118*, 1150–1154. [[CrossRef](#)]
19. Raghavan, B.; Gupta, T. H₂/CH₄ Gas Separation by Variation in Pore Geometry of Nanoporous Graphene. *J. Phys. Chem. C* **2017**, *121*, 1904–1909. [[CrossRef](#)]
20. Liu, H.; Chen, Z.; Dai, S.; Jiang, D. Selectivity trend of gas separation through nanoporous graphene. *J. Solid State Chem.* **2015**, *224*, 2–6. [[CrossRef](#)]
21. Coasne, B.; Jain, S.K.; Naamar, L.; Gubbins, K.E. Freezing of argon in ordered and disordered porous carbon. *Phys. Rev. B* **2007**, *76*, 085416. [[CrossRef](#)]

22. Jin, D.; Zhong, J. Melting Point of a Confined Fluid within Nanopores: The Composition Effect on the Gibbs-Thomson Equation. *J. Phys. Chem. B* **2023**, *127*, 5295–5307. [[CrossRef](#)] [[PubMed](#)]
23. Frenkel, D.; Smit, B. *Understanding Molecular Simulation: From Algorithms to Applications*, 2nd ed.; Academic Press: San Diego, CA, USA, 2002; pp. 23–61.
24. Li, W.; Zheng, X.; Dong, Z.; Li, C.; Wang, W.; Yan, Y.; Zhang, J. Molecular Dynamics Simulations of CO₂/N₂ Separation through Two-Dimensional Graphene Oxide Membranes. *J. Phys. Chem. C* **2016**, *120*, 26061–26066. [[CrossRef](#)]
25. Koosha, N.; KarimI-Sabet, J.; Moosavian, M.A.; Amini, Y. Improvement of synthesized graphene structure through various solvent liquids at low temperatures by chemical vapor deposition method. *Mater. Sci. Eng. B* **2021**, *274*, 115458. [[CrossRef](#)]
26. Bond, S.D.; Leimkuhler, B.J. Stabilized Integration of Hamiltonian Systems with Hard-Sphere Inequality Constraints. *Siam. J. Sci. Comput.* **2008**, *30*, 134–147. [[CrossRef](#)]
27. Jin, D.; Lu, X.; Zhang, M.; Wei, S.; Zhu, Q.; Shi, X.; Shao, Y.; Wang, W.; Guo, W. The adsorption behaviour of CH₄ on microporous carbons: Effects of surface heterogeneity. *Phys. Chem. Chem. Phys.* **2014**, *16*, 11037–11046. [[CrossRef](#)]
28. Plimpton, S. Fast Parallel Algorithms for Short-Range Molecular Dynamics. *J. Comput. Phys.* **1995**, *117*, 1–19. [[CrossRef](#)]
29. Hoover, W.G. Canonical dynamics: Equilibrium phase-space distributions. *Phys. Rev. A* **1985**, *31*, 1695–1697. [[CrossRef](#)]
30. Nosé, S. A unified formulation of the constant temperature molecular dynamics methods. *J. Chem. Phys.* **1984**, *81*, 511–519. [[CrossRef](#)]
31. Sang, P.; Zhao, L.; Xu, J.; Shi, Z.; Guo, S.; Yu, Y.; Zhu, H.; Yan, Z.; Guo, W. Excellent membranes for hydrogen purification: Dumbbell-shaped porous γ -graphynes. *Int. J. Hydrogen Energy* **2017**, *42*, 5168–5176. [[CrossRef](#)]
32. Lu, X.; Jin, D.; Wei, S.; Zhang, M.; Zhu, Q.; Shi, X.; Deng, Z.; Guo, W.; Shen, W. Competitive adsorption of a binary CO₂-CH₄ mixture in nanoporous carbons: Effects of edge-functionalization. *Nanoscale* **2015**, *7*, 1002–1012. [[CrossRef](#)] [[PubMed](#)]
33. Ghosvandi, S.; Coasne, B.; Clatworthy, E.B.; Guillet-Nicolas, R.; Bazin, P.; Desmurs, M.; Jacobo Aguilera, L.; Ruaux, V.; Mintova, S. Alkali Metal Cations Influence the CO₂ Adsorption Capacity of Nanosized Chabazite: Modeling vs Experiment. *ACS Appl. Nano Mater.* **2022**, *5*, 5578–5588. [[CrossRef](#)]
34. Jiao, S.; Xu, Z. Selective gas diffusion in graphene oxides membranes: A molecular dynamics simulations study. *ACS Appl. Mater. Interfaces* **2015**, *7*, 9052–9059. [[CrossRef](#)] [[PubMed](#)]
35. Simões, A.; Costa, E. Prediction in evolutionary algorithms for dynamic environments using markov chains and nonlinear regression. In Proceedings of the 11th Annual Conference on Genetic and Evolutionary Computation, Montreal, QC, Canada, 28 May 2019; pp. 883–890.
36. Hernandez, M.I.; Bartolomei, M.; Campos-Martinez, J. Transmission of Helium Isotopes through Graphdiyne Pores: Tunneling versus Zero Point Energy Effects. *J. Phys. Chem. A* **2015**, *119*, 10743–10749. [[CrossRef](#)]
37. Mandra, S.; Schrier, J.; Ceotto, M. Helium isotope enrichment by resonant tunneling through nanoporous graphene bilayers. *J. Phys. Chem. A* **2014**, *118*, 6457–6465. [[CrossRef](#)]
38. Schrier, J.; McClain, J. Thermally-driven isotope separation across nanoporous graphene. *Chem. Phys. Lett.* **2012**, *521*, 118–124. [[CrossRef](#)]
39. Jin, D.; Coasne, B. Molecular Simulation of the Phase Diagram of Methane Hydrate: Free Energy Calculations, Direct Coexistence Method, and Hyperparallel Tempering. *Langmuir* **2017**, *33*, 11217–11230. [[CrossRef](#)]
40. Lee, T.; Bocquet, L.; Coasne, B. Activated desorption at heterogeneous interfaces and long-time kinetics of hydrocarbon recovery from nanoporous media. *Nat. Commun.* **2016**, *7*, 11890. [[CrossRef](#)]
41. Shi, Y.; Hao, Y.; Wang, D.; Zhang, J.; Zhang, P.; Shi, X.; Han, D.; Chai, Z.; Yan, J. Effects of the flow rate of hydrogen on the growth of graphene. *Int. J. Min. Met. Mater.* **2015**, *22*, 102–110. [[CrossRef](#)]
42. Azamat, J.; Baghbani, N.B.; Erfan-Niya, H. Atomistic understanding of functionalized γ -graphyne-1 nanosheet membranes for water desalination. *J. Membr. Sci.* **2020**, *604*, 118079. [[CrossRef](#)]
43. Zhang, W.; Xu, Z.; Yang, X. Molecular simulation of penetration separation for ethanol/water mixtures using two-dimensional nanoweb graphynes. *Chin. J. Chem. Eng.* **2019**, *27*, 286–292. [[CrossRef](#)]
44. Kobashi, K.; Yoon, H.; Ata, S.; Yamada, T.; Futaba, D.N.; Hata, K. Designing Neat and Composite Carbon Nanotube Materials by Porosimetric Characterization. *Nanoscale Res. Lett.* **2017**, *12*, 616. [[CrossRef](#)] [[PubMed](#)]
45. Cai, W.; Wang, M.; Yang, G.Q.; Zhang, Z.; Wang, Y.; Li, J. Study of the Dissolution and Diffusion of Propane, Propylene and Nitrogen in Polydimethylsiloxane Membranes with Molecular Dynamics Simulation and Monte Carlo Simulation. *Separations* **2022**, *9*, 116. [[CrossRef](#)]
46. Guo, M.; Zhang, Y.; Xu, R.; Ren, X.; Huang, W.; Zhong, J.; Tsuru, T.; Kanezashi, M. Ultrahigh permeation of CO₂ capture using composite organosilica membranes. *Sep. Purif. Technol.* **2022**, *282*, 120061. [[CrossRef](#)]

Disclaimer/Publisher's Note: The statements, opinions and data contained in all publications are solely those of the individual author(s) and contributor(s) and not of MDPI and/or the editor(s). MDPI and/or the editor(s) disclaim responsibility for any injury to people or property resulting from any ideas, methods, instructions or products referred to in the content.